Eur. Phys. J. B (2011)
DOI: 10.1140/epjb/e2011-20313-9

THE EUROPEAN PHYSICAL JOURNAL B

Regular Article

Electronic transport properties of junctions between carbon nanotubes and graphene nanoribbons

K.L. Ma[1], X.H. Yan[1,2,a], Y.D. Guo[1], and Y. Xiao[1]

[1] College of Science, Nanjing University of Aeronautics and Astronautics, Nanjing 211106, P.R. China
[2] School of Electronic Science & Engineering, Nanjing University of Post and Telecommunications, Nanjing 210046, P.R. China

Received 24 April 2011 / Received in final form 7 September 2011
Published online 24 October 2011 –

Abstract. Using the tight-binding model and Green's function method, we studied the electronic transport of four kinds of nanotube-graphene junctions. The results show the transport properties depend on both types of the carbon nanotube and graphene nanoribbon, metal or semiconducting. Moreover, the defect at the nanotube-graphene interface did not affect the conductance of the whole system at the Fermi level. In the double junction of nanotube/nanoribbon/nanotube, quasibound states are found, which cause antiresonance and result in conductance dips.

1 Introduction

Carbon nanotube (CNT) and graphene nanoribbon (GNR) are promising candidates for the next-generation of nanoelectronic devices due to their peculiar electronic properties [1–6]. The transport properties of junctions formed by CNT/CNT [7–9] or GNR/GNR [10–13] have been widely studied both in theory and experiment. And many interesting phenomena have been observed, e.g., transmission resonating [14] and rectification [15].

Recently, much attention has been paid to the CNT/GNR junction, which can be constructed by different types of CNT and GNR. The CNT/GNR junction can be fabricated in high yields through three methods, i.e., chemical attack [16], plasmaetching [17], and lithium intercalation followed by exfoliation [18]. In theory, Santos et al. [19] found the metallic CNT/GNR junction is a magnetoresistive device. Li et al. [20] studied the electronic and transport properties of CNT/GNR hybrids with a transverse electric field and found the conductance strongly depend on the field strength. Besides, Klymenko [21] found the ballistic transport through GNR/CNT/GNR can be considered as the result of Fabry-Perot interference between the two GNR/CNT interfaces. All these studies open a new route for the design of mixed CNT/GNR devices. However, the electronic transport properties of semiconducting CNT/GNR junctions, especially formed by different CNT and GNR, have been less reported. Also, the double junction, such as ACNT/ZGNR/ACNT, need to be further studied. In the present work, we theoretically studied the electronic transport of four kinds of CNT/GNR junctions, i.e., metal-metal (MM), semiconductor-semiconductor (SS), semiconductor-metal (SM), and metal-semiconductor (MS) junctions. All these CNT/GNR junctions can be achieved by cutting the CNT in experiment. Furthermore, we also studied the electronic transport of ACNT/ZGNR/ACNT junction.

2 Model and methods

The CNT can be described by the parameters of m and n [22]. There are three types of CNT according to their structures, i.e., armchair CNT (ACNT with $m = n$), zigzag CNT (ZCNT with $n = 0$) and chiral CNT ($m \neq n$ and $n \neq 0$). The GNR with finite width can be divided into zigzag GNR (ZGNR) and armchair GNR (AGNR) according to the atomic arrangement pattern on their edges.

The geometry of CNT/GNR junctions (a semi-infinite CNT is connected to a semi-infinite GNR) is shown in Figure 1 [(a) ACNT/ZGNR junction and (b) ZCNT/AGNR junction]. There is no defect at the contact interface, as the CNT/GNR junction can be regard as an unzipped CNT. ACNT/ZGNR and ZCNT/AGNR junctions are described by (n, n)ACNT/$2n$-ZGNR and $(n, 0)$ZCNT/$2n$-AGNR, respectively, where $2n$ is the number of carbon atoms of CNT circumference or the number of carbon atoms of GNR in the unit cell (Fig. 1).

The calculation is based on the well-known Green's function method and the tight-binding methodology. The tight-binding methodology only considers the interaction between nearest neighbors and neglects other ones. Besides, it ignores the electron interaction and only describes the electron structure approximatively. But the tight-binding methodology shows great advantage in describing the electronic transport of quasi-one-dimensional

[a] e-mail: xhyan@nuaa.edu.cn

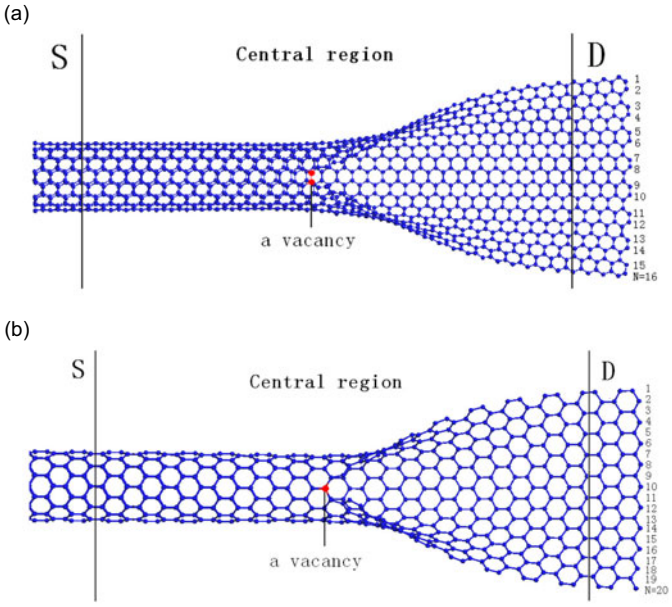

Fig. 1. (Color online) Geometry of junctions for (a) ACNT/ZGNR and (b) ZCNT/AGNR, which include the source, drain, and the central region.

system and has been widely used in CNT and GNR systems [14,23,24]. The advantage of using a tight-binding model resides in its simplicity, the general features of electronic transport being in very good agreement with those obtained by more sophisticated approaches [25].

We divide the system into three parts: a semi-infinite CNT lead [labeled by S (source)], a semi-infinite GNR lead [labeled by D (drain)], and the central region (Fig. 1). For a tight-binding model of CNT/GNR with one π-electron per carbon atom, the spinless Hamiltonian is

$$H = \sum_i \varepsilon_i c_i^\dagger c_i - t \sum_{\langle i,j \rangle} \left(c_i^\dagger c_j + h.c. \right), \tag{1}$$

where ε_i is the on-site energy, t is the nearest-neighbor hopping energy, and $c_i^\dagger(c_i)$ creates (annihilates) an electron on the site i. The sum in $\langle i,j \rangle$ is restricted to the nearest-neighbor atom pairs. In our calculations, t is set to be 2.66 eV [23] and ε_i is zero [23]. The effect of unzipping is equal to cutting the hopping between the carbon atoms where the opening occurs, and assume the unzipping does not modify the hopping between the other carbon atoms [19].

Based on the Hamiltonian, we calculate the electronic conductance of the CNT/GNR junction with the lattice Green's function method [26]. The total Green's function can be expressed as [26]

$$G(E) = \left[E - H - \Sigma_S - \Sigma_D \right]^{-1}, \tag{2}$$

where H is the Hamiltonian of central region and $\Sigma_{S,D} = H_1^\dagger G_{S,D} H_1$ is the self-energy of the source or drain leads. H_1 is the interaction matrix between the source (drain) and the central region. $G_{S,D}$ is the Green's function of the source or drain leads, which can be calculated by the recursive Green's function technique [27]. After the total Green's function is obtained, the zero-temperature conductance (C) and the local density of states (LDOS, denoted by L) of a junction can be calculated by [26]

$$C(E) = G_0 \mathrm{Tr}[\Gamma_S(E) G^\dagger(E) \Gamma_D(E) G(E)] \tag{3}$$

and

$$L(E) = -\mathrm{ImTrace}[C(E)]/\pi, \tag{4}$$

where $\Gamma_{S,D} = i[\Sigma_{S,D} - \Sigma_{S,D}^\dagger]$ is the coupling function of the source or drain lead, and $G_0 = 2e^2/h$ is the conductance quantum.

3 Results and discussions

As is known, all the ZGNRs and AGNRs with width $N = 3n + 2$ are metallic, and others are semiconducting, where n is an integer [28]. A (m, n)CNT is metallic only if $m - n = 3k$ and others are semiconducting, where k is an integer. Based on these, we designed four junctions, i.e., (8, 8)ACNT/16-ZGNR, (11, 0)ZCNT/22-AGNR, (10, 0)ZCNT/20-AGNR, and (12, 0)ZCNT/24-AGNR. They are MM, SS, SM, and MS junctions, respectively. In our calculations, curvature effects are not considered, as they are not significant when the diameter of CNT is large enough [29,30].

Figure 2 shows the conductance as a function of electron energy E for the CNT/GNR junction. As a reference, dashed (dotted) line for the conductance of the perfect infinite CNT (GNR) is also shown. The junction is metallic only when both of the CNT and GNR are metallic. Figure 2a shows the conductance of the MM junction, we can see that the junction is metallic and the conductance of the junction at the Fermi level is equal to that of the perfect ZGNR, which means the ACNT acts like a transparent contact for the ZGNR. From another viewpoint, ZGNR can lower the conductance of the ACNT at the Fermi level and make it equal to that of the perfect ZGNR, which demonstrates ZGNR behaves like a valley filter for the ACNT. For SS junction (Fig. 2b), it is semiconducting and the band gap (∼0.89 eV) is equal to that of the perfect ZCNT (∼0.89 eV), indicating AGNR also behaves like a transparent contact for ZCNT. In other words, ZCNT can enlarge the band gap of AGNR (∼0.43 eV) and make it equal to that of the perfect ZCNT. This feature can be used to change the band gap of AGNR by zipping AGNR. From Figure 2c, we can see the SM junction is semiconducting and the band gap (∼0.93 eV) is equal to that of ZCNT. Again, this feature can be used to modulate AGNR from metallic to semiconducting by zipping AGNR. And we can see the MS junction is also semiconducting (Fig. 2d) with the band gap (∼0.39 eV) being equal to that of the AGNR. Similarly, this can be used to modulate ZCNT from metallic to semiconducting by opening ZCNT. Previous studies have already shown that defects could affect the transport properties of CNT and GNR [31–33]. It reminds researchers that the defect may

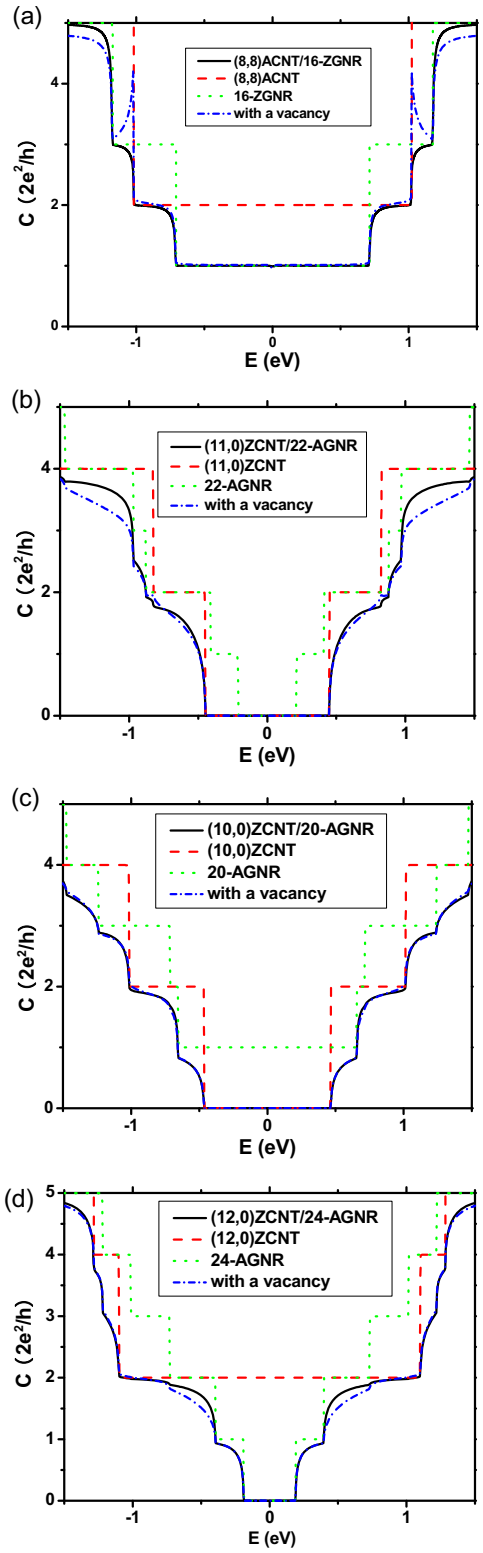

Fig. 2. (Color online) The conductance as a function of electron energy for (a) (8, 8)ACNT/16-ZGNR junction, (b) (11, 0)ZCNT/22-AGNR junction, (c) (10, 0)ZCNT/20-AGNR junction, and (d) (12, 0)ZCNT/24-AGNR junction. The solid and short dash dotted lines represent the conductance of perfect and defected CNT/GNR junctions, respectively. And the dash and dotted lines represent the conductance of CNT and GNR, respectively.

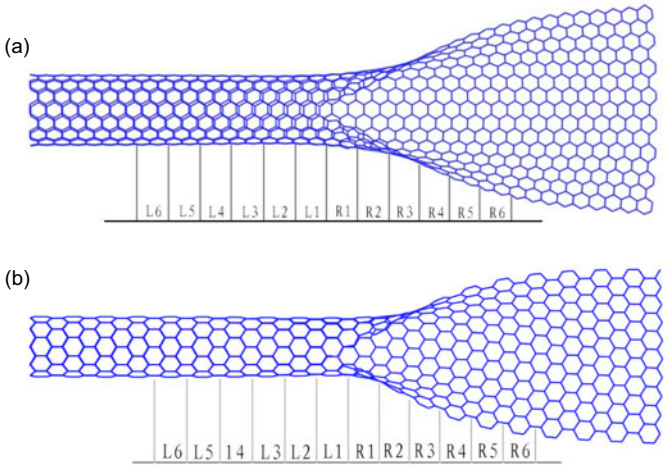

Fig. 3. (Color online) Geometry of spatial-resolved junctions for (a) ACNT/ZGNR junction and (b) ZCNT/AGNR junction.

play an important role in determining the transport properties of junctions. So we also studied the effect of a vacancy on the junction conductance. We place a vacancy at the interface (Fig. 1) for each junction. Figure 2 indicates that a single lattice vacancy can hardly affect the junction conductance at the Fermi level (-1 eV $< E <$ 1 eV), except the small weakening of conductance for MS junction in the energy range of 0.40 eV $< |E| <$ 0.73 eV. Previous studies showed that, the vacancy defect in metallic CNT will lower the conductance by one conductance quantum from 2 G_0 to 1 G_0 at the Fermi level (our defect is located at the CNT part). While, due to the presence of non-defected GNR, the conductance is already lowered to 1 G_0 at the Fermi level. As a result, the vacancy in the junction appears not to affect the conductance around the Fermi level.

In order to examining the detailed electronic structure of the junction, we analyzed the spatial-resolved LDOS. The atoms are grouped into slices denoted by Lx ($x = 1, 2, 3, \ldots$) according to the distance from the interface (Fig. 3). Here we choose the slice of 0.492 nm wide (a unit cell of the perfect ACNT or ZGNR) for ACNT/ZGNR and the slice of 0.426 nm wide (a unit cell of the perfect ZCNT or AGNR) for ZCNT/AGNR. The average LDOS for each slice is plotted in Figure 4. For MM junction (Fig. 4a), from the ACNT side we find the average LDOS of L3 is similar to that of perfect (8, 8)ACNT, especially the peak at $E = 0$ eV. And the average LDOS of L6 is quite similar to that of perfect (8, 8)ACNT. From the ZGNR side, we find the average LDOS of R3 is similar to that of perfect 16-ZGNR, especially the distance between the two peaks ($|E| = 1$ eV). And the average LDOS of R6 is quite similar to that of perfect 16-ZGNR. These results show that the attenuation length for both semi-infinite (8, 8)ACNT and semi-infinite 16-ZGNR in the MM junction is about 2.95 nm. For SS junction (Fig. 4b), the average LDOS of L6 is similar to that of perfect (11, 0)ZCNT, especially the distance between the two peaks ($|E| = 0.46$ eV). Besides, the average LDOS of R6 is similar to that of the perfect

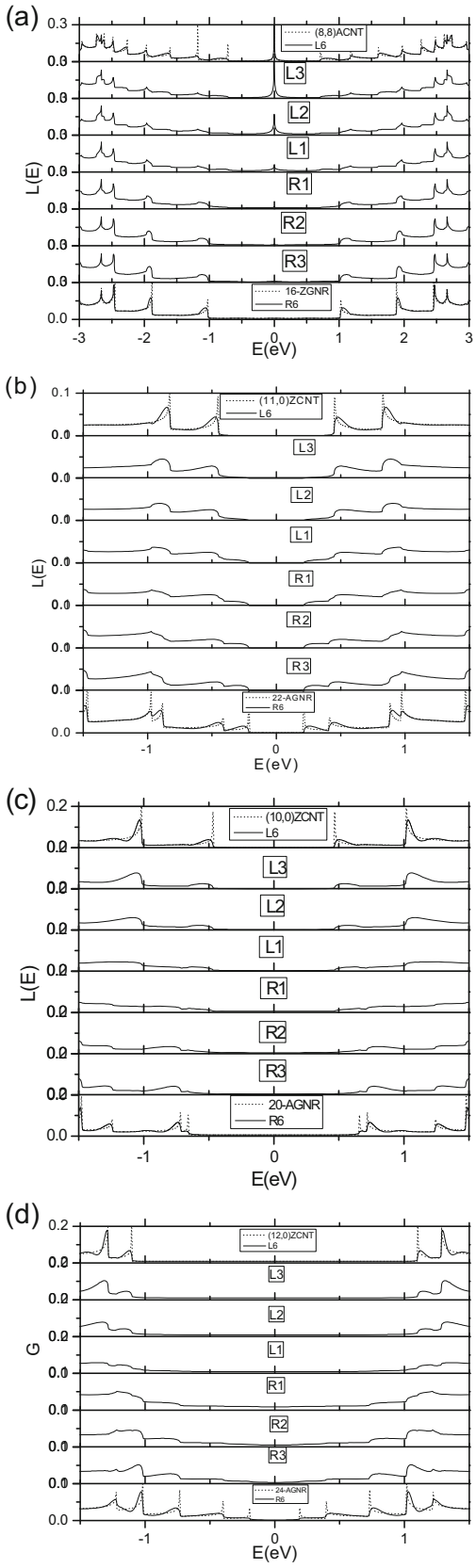

Fig. 4. The spatial-resolved LDOS for (a) (8, 8)ACNT/16-ZGNR junction, (b) (11, 0)ZCNT/22-AGNR junction, (c) (10, 0)ZCNT/20-AGNR junction, and (d) (12, 0)ZCNT/24-AGNR junction.

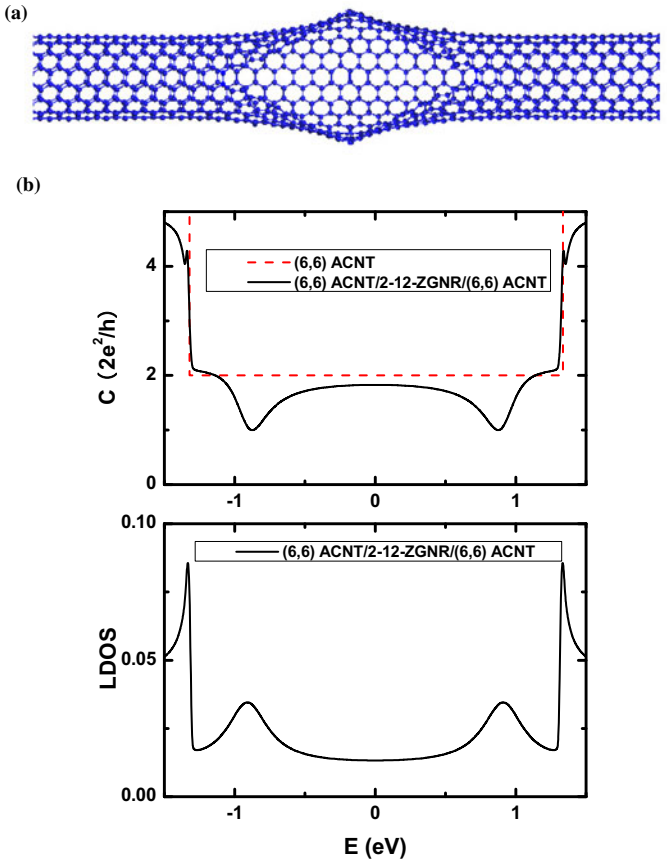

Fig. 5. (Color online) (a) Geometry of (n, n)ACNT/N-2n-ZGNR/(n, n)ACNT double junction, (b) The conductance (top) and the LDOS (bottom) as a function of electron energy for (6, 6)ACNT/2-12-ZGNR/(6, 6)ACNT.

22-AGNR, especially the distance between the two peaks ($|E| = 0.22$ eV). This time, the attenuation length for both semi-infinite (11, 0)ZCNT and semi-infinite 22-AGNR in the SS junction is about 2.556 nm. The cases of SM junction and MS junction are similar to that of SS junction, because all of them consist of semi-infinite ZCNT and AGNR.

Next, we explore the electronic transport properties of the double junction, such as the one in Figure 5a. It is formed by opening an infinite (n, n)ACNT in the center, denoted by (n, n)ACNT/N-2n-ZGNR/(n, n)ACNT, where N is the number of unit cells in the 2n-ZGNR, and 2n is the width of the ZGNR. New electronic transport properties are expected, as the finite 2n-ZGNR could be regard as a cavity. The conductance C of the double junction (6, 6)ACNT/2-12-ZGNR/(6, 6)ACNT versus energy E is shown in Figure 5b. The conductance of perfect (6, 6)ACNT near the Fermi level is equal to $2 \times 2e^2/h$. When (6, 6)ACNT opens a cavity, two conductance dips appear at $E = \pm 0.88$ eV (we name it dip-energy). In fact, these dips are associated with antiresonance caused by quasibound states in the finite 12-ZGNR. The LDOS of finite 12-ZGNR in (6, 6)ACNT/2-12-ZGNR/(6, 6)ACNT junction is plotted in Figure 5b (bottom). One can see

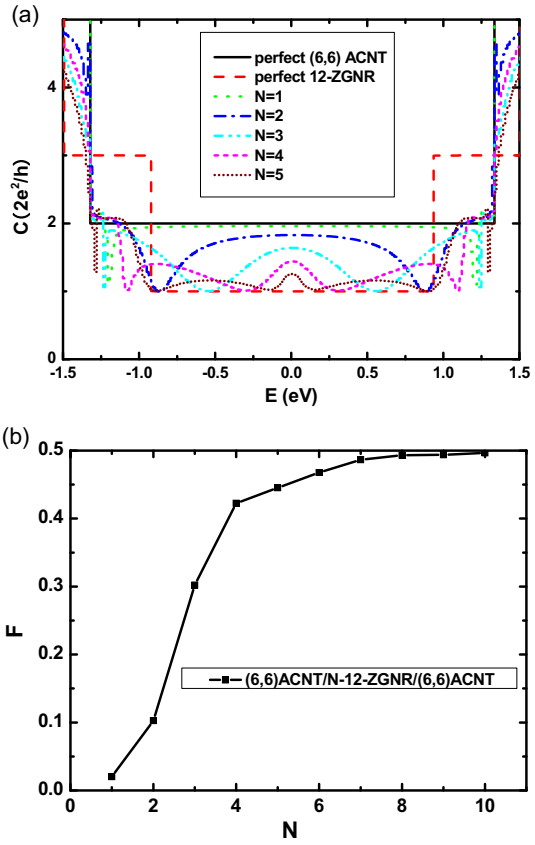

Fig. 6. (Color online) (a) The conductance as a function of electron energy and (b) the decreasing rate of the average conductance of (6, 6) ACNT/N-12-ZGNR/(6, 6)ACNT for several ZGNR lengths.

there are two peaks at the same energies $E = \pm 0.88$ eV, which indicate the existence of quasibound states in the finite 2-12-ZGNR. Obviously, it is the quasibound states in the finite 12-ZGNR that cause antiresonance and result in the conductance dips. We next discuss the reason why the quasibound states appear. Actually, the whole junction of (6, 6)ACNT/2-12-ZGNR/(6, 6)ACNT can be seen as a big defect in the (6, 6)ACNT. The whole junction was achieved by cutting several hopping between the carbon atoms in the center of perfect (6, 6)ACNT in the calculating method. As a result, the region of the center, i.e., 2-12-ZGNR, could be regarded as a defect for the perfect (6, 6)ACNT. It is this defect that leads to the quasibound states, and then causes antiresonance and results in the conductance dip.

The conductance of (6, 6)ACNT/N-12-ZGNR/(6, 6)ACNT for different N is shown in Figure 6a. Compared with the perfect (6, 6)CNT, the quantum step feature disappears and the conductance decreases overall with some dips appearing ($|E| = 1.21$, 0.88, 0.55, 0.31, 0.15 eV). Besides, with the increase of N, the dip-energy decreases (from 1.21 to 0.15 eV) and the conductance near the Fermi level decreases and gradually approaches to the case of perfect 12-ZGNR ($2e^2/h$). The ZGNR (long enough) behaves like a valley filter for the ACNT, lower its conductance at the Fermi level, and make it equal to that of the perfect ZGNR, like the analyzing above in MM junction. When N increases, more dips appear, e.g., $|E| = 1.24$ eV ($N = 3$), $|E| = 1.09$ eV ($N = 4$), and $|E| = 1.29$, 0.89 eV ($N = 5$), inducing more quasibound states.

In order to quantitatively study the effect of the length N on the conductance near the Fermi level, we compute the decreasing rate of the average conductance [34]

$$F = \frac{\overline{\Delta C}}{\overline{C_{CNT}}} = \frac{\int_{-\Delta E}^{\Delta E} [C_{CNT}(E) - C(E)]\, dE}{\int_{-\Delta E}^{\Delta E} C_{CNT}(E) dE}, \qquad (5)$$

where $C_{CNT}(E)$ and $C(E)$ are the conductance of the (6, 6)ACNT and (6, 6)ACNT/N-12-ZGNR/(6, 6)ACNT junction, respectively ($\Delta E = 0.5$ eV in our calculations). Figure 6b shows the decreasing rate of the average conductance varying with N. One can see that, as the ZGNR length N increases, the decreasing rate of the average conductance F increases from about 0.02 ($N = 1$) to about 0.5 ($N = 10$). So the conductance of the double junction near the Fermi level will be very close to that of the perfect 12-ZGNR when $N = 10$.

4 Conclusions

We have theoretically studied the electronic transport properties of four kinds of junctions constructed from different carbon nanotubes and graphene nanoribbons using the tight-binding model and Green's function method. The results show that the electronic transport properties depend on both of the carbon nanotubes and graphene nanoribbons. Moreover, the conductance of junctions near the Fermi level is found to be robust to the defect. Double junction of ACNT/ZGNR/ACNT was also studied and quasibound states were found, which can cause antiresonance and then result in the conductance dips. We believed these features will be very useful for designing future nanoelectronic devices.

This work was supported by the National Natural Science Foundation of China (NSFC10874089 and NSFC51032002), the key project of National High Technology Research and Development Program of China (2011AA050526), Funding of Jiangsu Innovation Program for Graduate Education (CXZZ11_0190), and Natural Science Foundation of Jiangsu Province of China (BK2008398).

References

1. S. Iijima, Nature **354**, 56 (1991)
2. K. Novoselov, A. Geim, S. Morozov, D. Jiang, Y. Zhang, S. Dubonos, I. Grigorieva, A. Firsov, Science **306**, 666 (2004)
3. A. Bachtold, P. Hadley, T. Nakanishi, C. Dekker, Science **294**, 1317 (2001)
4. S. Tans, A. Verschueren, C. Dekker, Nature **393**, 49 (1998)

5. B. Trauzettel, D. Bulaev, D. Loss, G. Burkard, Nature Physics **3**, 192 (2007)
6. X. Wang, Y. Ouyang, X. Li, H. Wang, J. Guo, H. Dai, Phys. Rev. Lett. **100**, 206803 (2008)
7. M. Ouyang, J. Huang, C. Cheung, C. Lieber, Science **291**, 97 (2001)
8. M. Menon, A. Andriotis, D. Srivastava, I. Ponomareva, L. Chernozatonskii, Phys. Rev. Lett. **91**, 145501 (2003)
9. A. Andriotis, M. Menon, D. Srivastava, L. Chernozatonskii, Phys. Rev. B **65**, 165416 (2002)
10. H. Li, L. Wang, Y. Zheng, J. Appl. Phys. **105**, 013703 (2009)
11. S. Hong, Y. Yoon, J. Guo, Appl. Phys. Lett. **92**, 083107 (2008)
12. Z. Xu, Q.S. Zheng, G. Chen, Appl. Phys. Lett. **90**, 223115 (2007)
13. A.N. Andriotis, E. Richter, M. Menon, Appl. Phys. Lett. **91**, 152105 (2007)
14. E. Jódar, A. Pérez-Garrido, A. Díaz-Sánchez, Phys. Rev. B **73**, 205403 (2006)
15. A. Andriotis, M. Menon, D. Srivastava, L. Chernozatonskii, Phys. Rev. Lett. **87**, 66802 (2001)
16. A.G. Cano-Marquez, F.J. Rodríguez-Macias, J. Campos-Delgado, C.G. Espinosa-Gonzalez, F. Tristan-Lopez, D. Ramírez-Gonzalez, D.A. Cullen, D.J. Smith, M. Terrones, Y.I. Vega-Cantu, Nano, Lett. **9**, 1527 (2009)
17. D.V. Kosynkin, A.L. Higginbotham, A. Sinitskii, J.R. Lomeda, A. Dimiev, B.K. Price, J.M. Tour, Nature **458**, 872 (2009)
18. L. Jiao, L. Zhang, X. Wang, G. Diankov, H. Dai, Nature **458**, 877 (2009)
19. H. Santos, L. Chico, L. Brey, Phys. Rev. Lett. **103**, 86801 (2009)
20. T. Li, S. Chang, M. Lin, Eur. Phys. J. B **70**, 497 (2009)
21. Y.O. Klymenko, Eur. Phys. J. B **77**, 443 (2010)
22. R. Saito, M. Fujita, G. Dresselhaus, M. Dresselhaus, Phys. Rev. B **46**, 1804 (1992)
23. L. Chico, L.X. Benedict, S.G. Louie, M.L. Cohen, Phys. Rev. B **54**, 2600 (1996)
24. K.L. Ma, X.H Yan, Y. Xiao, Y.P. Chen, Solid State Commun. **150**, 1308 (2010)
25. D. Orlikowski, H. Mehrez, J. Taylor, H. Guo, J. Wang, C. Roland, Phys. Rev. B **63**, 155412 (2001)
26. S. Datta, *Electronic Transport in Mesoscopic Systems* (Cambridge University Press, 1997)
27. F. Sols, M. Macucci, U. Ravaioli, K. Hess, J. Appl. Phys. **66**, 3892 (1989)
28. K. Nakada, M. Fujita, G. Dresselhaus, M. Dresselhaus, Phys. Rev. B **54**, 17954 (1996)
29. X. Blase, L.X. Benedict, E.L. Shirley, S.G. Louie, Phys. Rev. Lett. **72**, 1878 (1994)
30. V. Zólyomi, J. Kürti, Phys. Rev. B **70**, 85403 (2004)
31. I. Deretzis, A. La Magna, Eur. Phys. J. B **81**, 15 (2011)
32. H. Joon, J. Ihm, S.G. Louie, M.L. Cohen, Phys. Rev. Lett. **84**, 2917 (2000)
33. I. Deretzis, G. Fiori, G. Iannaccone, A. La Magna, Phys. Rev. B **81**, 085427 (2010)
34. T. Li, S.P. Lu, Phys. Rev. B **77**, 085408 (2008)